

# Catalytic Extraction of Microcrystalline Cellulose (MCC) from *Elaeis guineensis* using Central Composite Design (CCD)

Sharifah Bee Abd Hamid\*, Zaira Zaman Chowdhury, and Md. Ziaul Karim

Cellulosic fiber extracted from a non-woody, monocotyledonous species of palm tree trunk (PTT) was hydrolyzed with different concentrations of  $\text{FeCl}_3$  in the presence of hydrochloric acid. The dissolution properties of the amorphous region of palm tree cellulosic fiber (PTC) can be enhanced in the presence of  $\text{Fe}^{3+}$  cations in acidic medium. The independent variables, including temperature ( $x_1$ ), time ( $x_2$ ), and concentration of metal chloride ( $\text{FeCl}_3$ ) catalyst ( $x_3$ ), were optimized using central composite design (CCD). Responses were measured in terms of percentage crystallinity ( $y_1$ ) and yield ( $y_2$ ) of the prepared hydrocellulose. Analysis of variance (ANOVA) showed that temperature was the most influential factor for hydrolyzing the amorphous sections of cellulose. Under optimum conditions, the percentage crystallinity ( $y_1$ ) and yield ( $y_2$ ) were 68.66% and 83.98%, respectively. Scanning electron microscopy (SEM) analysis and X-ray diffraction techniques were used to obtain more information about the surface morphology and crystallinity of the prepared microcrystalline cellulose (MCC). Infrared spectroscopy and thermal analysis were performed to observe the effect of hydrolysis on the finished products. It was concluded that the addition of  $\text{FeCl}_3$  salt in acid hydrolyzing medium can substantially increase the crystallinity of palm tree trunk cellulose with significant morphological changes to yield microcrystalline cellulose (MCC).

*Keywords:* Palm tree cellulose (PTC); Microcrystalline cellulose (MCC); Hydrocellulose; Central composite design (CCD); Percentage crystallinity; Amorphous sections

*Contact information:* Nanotechnology and Catalysis Center (NANOCAT), University Malaya, Kuala Lumpur 50603, Malaysia; \*Corresponding author: sharifahbee@um.edu.my

## INTRODUCTION

Recently, research has focused on obtaining sustainable, green, and ecofriendly materials for versatile applications (Abdul Khalil *et al.* 2012; Khalil *et al.* 2013). Cellulose, the main component of all biomass, is the most abundant bio-macromolecule found in nature. It has been estimated that more than  $7.5 \times 10^{10}$  tons of cellulose is produced annually (Habibi *et al.* 2010). Irrespective of biomass sources, the long-chain cellulose polymer consists of a linear homo-polysaccharide composed of d-glucopyranose units linked together by 1-4 linkages. The repeating unit of cellulose is the dimer of glucose, known as cellubiose (Moon *et al.* 2011; Chowdhury *et al.* 2014). In addition to biodegradability and renewability, the fabrication of cellulosic materials into micro as well as nano dimensions enhances favorable characteristics such as excellent mechanical properties, high crystallinity, and low molecular weight (de Mesquita *et al.* 2010). Preparation of microcrystalline cellulose (MCC) derived from renewable sources is presently a hot investigation area. Microcrystalline cellulose, a porous, non-fibrous, white, odorless, purified, crystalline powder, is perhaps the best filler-binder used currently for pharmaceutical products (Ejikeme 2008; Li *et al.* 2013). It has been extracted by partial

de-polymerization of native cellulose *via* hydrolysis with dilute mineral acids or enzymolysis (Ejikeme 2008). However, the acid extraction process is popular for industrial scale preparation of MCC due to its lower price and desirable properties of high crystallinity (Adel *et al.* 2011; Li *et al.* 2014).

The degree of crystallinity observed after hydrolysis of native cellulose is very important because it affects several properties, including compactibility, stabilizing capability for suspension, and water retention ability of MCC particles. Subsequently, this influences the flow ability of the MCC particles used as excipients or filler for final medicinal products (Azubuike *et al.* 2012). Because of its insoluble nature in common reagents like water, organic solvents, and dilute acids as well as its lubricating and hygroscopic properties, MCC has been widely used in cosmetics and the food industry as a fat replacement (Omaray and Omaray 1986; Uesu *et al.* 2000). Furthermore, it is used for pelletisation during the direct compression method as well as dry and wet formulation of capsules (Rowe *et al.* 2006). The chemical composition and morphological features of MCC significantly depends on the characteristics of the raw cellulosic materials and the extent and type of processing variables (Landin *et al.* 1993). Because cellulose is extracted from different origins such as soft wood, hard wood, or non-woody lignocellulosic residues and has diversified properties such as crystallinity, moisture content, surface area, porous structure, and molecular weight, it is expected that MCC procured from unlike sources would exhibit different properties. Basically, excipient materials like MCC for oral drugs are preselected depending on their compatibility and functionality to ensure the constancy and bioavailability of the finished pharmaceutical products; at the same time, the material used should have the prospect for industrial scale production. Thus, from an economic viewpoint, the use of biomass residues to extract cellulosic fiber and transforming them to MCC particles is advantageous.

Microcrystalline cellulose particles have previously been produced from hard wood pulp like *Eucalyptus* (Li *et al.* 2013), soft wood of Norway spruce (Bondeson *et al.* 2006), and cotton linters (Nada *et al.* 2009). However, some other non-woody biomass, such as soybean, corn stalk, oat, rice hulls, sugar beet pulp (Hanna *et al.* 2001; Adel *et al.* 2011), bagasse, maize cob (Okhamafe and Azubuike 1994; Okhamafe *et al.* 1995), wheat, barley, oat straw (Proenca 1999), groundnut shell, rice husks (Okhamafe *et al.* 1991), reed stalks (Saleh and El-Ashmawy 1978), cereal straw (Jain *et al.* 1983), Indian bamboo (Ofoefule and Chukwu 1999), and *Luffa cylindrica* (Ohwoavworhua *et al.* 2004), have also been recognized as potential sources of MCC. During acid hydrolysis of cellulosic materials, amorphous regions are fragmented, resulting in a highly crystalline substrate (Costa *et al.* 2011). The amorphous regions are selectively hydrolyzed by strong mineral acids such as hydrochloric, nitric, and sulfuric acids (Follain *et al.* 2010; Hashaikeh and Abushammala 2011). However, to degrade the amorphous regions of cellulose while retaining the crystalline region almost unaltered to enhance the yield and crystallinity of MCC is challenging. Lack of process parameter optimization may result in char formation with drastic degradation of cellulosic backbone to yield other organic compounds as by-products rather than MCC particles. In this context, previous researchers have used different types of transition metal salts as catalysts such as FeCl<sub>3</sub>, CuCl<sub>2</sub>, and AlCl<sub>3</sub> during acid hydrolysis of cellulose (Kamireddy *et al.* 2013). It was reported that a minute amount of FeSO<sub>4</sub> can enhance the reducing sugar content during the hydrolysis of coniferous sawdust (Ren *et al.* 2012). Previous findings show that hydrolysis efficiency of cellulose can be upgraded significantly by the presence of Fe<sup>3+</sup> and H<sup>+</sup> ions simultaneously in the reaction medium (Sulaiman *et al.* 2012; Li *et al.* 2013).

Oil palm is considered to be a monocotyledonous, non-woody type of plant. The anatomical features of oil palm trunk differ chemically from hardwood and softwood species in terms of cellulose, hemicellulose, and lignin content (Akmar and Kennedy 2001; Nguyen and Tucker 2002; Dungani *et al.* 2013). The objective of this study was to hydrolyze the palm tree trunk cellulose (PTC) in the presence of  $\text{FeCl}_3$  catalyst during the acid hydrolysis process using response surface methodology (RSM). Central composite design (CCD) based on RSM is a combination of mathematical and statistical analysis of experimental observations. In the case of the conventional method, there is an amendment of only one parameter at a certain time interval while keeping the other parameters constant. Thus, a collective effect of all the parameters at a fixed time cannot be observed. This method is also time consuming and needs a lot of experiments for optimization. The RSM technique reduces process variability with accurate observation of output responses using a lesser number of experiments. This can establish an empirical relationship between the process variables with the desired responses or product characteristics. It delivers a complete experimental design for data assessment, model fitting, as well as a method for optimization (Chowdhury *et al.* 2011; 2012). Three individual factors of temperature, time, and concentration of metal ion catalyst were selected to investigate the hydrolysis mechanism of PTC in hydrochloric acid medium. The responses selected were percentage crystallinity of the hydrocellulose (MCC) and yield. Corresponding mathematical models were proposed. The effect of process variables on both the responses were analyzed in terms of analysis of variance (ANOVA).

## EXPERIMENTAL

### Materials

#### *Catalytic hydrolysis of palm tree cellulose (PTC)*

Palm tree cellulosic fiber (PTC) was supplied by the Malaysian Palm Oil Board (MPOB). It was procured from palm tree trunk biomass by the alkaline peroxide bleaching process (Mandal and Chakrabarty 2011). The dried and ground palm tree trunk was refluxed with 1 M sodium hydroxide solution for 8 h, where liquor to trunk ratio was 1:50 at room temperature. After alkali treatment, the residue contains 49.76% of cellulose, 8.5% hemicellulose, and 16.54% of lignin. It was bleached using 0.7% sodium chlorite solution (w/v) for 5 h. The reaction was carried out at pH 4 by adding buffer solution. After filtration, the delignified residue was washed with distilled water and boiled for 5 h with 5% sodium sulfite solution (w/v) to remove hemicellulose and lignin. The sample was further boiled with 17.5% sodium hydroxide solution for 5 h. The solution was filtered and the residue was washed and air dried; 50 mL of dimethylsulfoxide (DMSO) was added to the dried sample in a water bath for 3 h at 80 °C. Finally the product was filtered, washed with distilled water, and air-dried. The chemical composition of palm tree trunk, alkali-pretreated trunk, and the obtained bleached cellulosic sample, provided by MPOB, is enlisted in Table 1.

Iron (III) chloride hexahydrate and hydrochloric acid fuming 37% were of analytical grade and purchased from R & M Chemicals and Merck, respectively. The PTC was treated by varying the concentration of  $\text{FeCl}_3$  based on a basic design matrix (Table 2) whereby the solid liquid ratio was kept constant (1:30) in the presence of HCl (3 M). The cellulose sample with requisite amount of acid and catalyst were placed in a 100-mL round bottom flask and stirred on a magnetic hot plate. The flasks were heated to various

temperatures and reaction times in a constant temperature oil bath. Samples were withdrawn from the reaction mixture under different reaction conditions preset by the experimental design (Tables 1 and 2).

**Table 1.** Chemical Composition of Palm Tree Trunk, Alkali-Pretreated Trunk, and Bleached Cellulosic Sample (PTC)

Palm Tree Trunk Sample	% Cellulose	% Hemicellulose	% Lignin	% Ash
Raw Trunk sample	39.87	25.79	28.98	5.36
Alkali Pretreated Trunk sample	59.88	17.67	15.22	7.23
Bleached Cellulosic Sample	88.03	1.05	0.89	8.09

The solution was centrifuged at 6000 rpm and washed with distilled deionized water until the filtrate was neutral. The sample was dried and the yield was calculated according to Eq. (1) (Li *et al.* 2013):

$$\% \text{ Yield} = \frac{w_t}{w_0} \times 100 \quad (1)$$

Here,  $w_t$  is the initial weight of PTC sample taken and  $w_0$  is the dry weight of powder finally obtained (Li *et al.* 2013).

## Methods

### *Central composite design (CCD)*

A two-level factorial design based on CCD using response surface methodology (RSM) was used to optimize the catalytic acid hydrolysis of PTC. This gives main and combined effects of variables on the responses under consideration. It also develops regression models with consequent optimization of the hydrolysis process. The influence of three independent variables,  $x_1$  (temperature),  $x_2$  (time), and  $x_3$  (concentration of  $\text{FeCl}_3$  catalyst), on two responses of percentage crystallinity ( $y_1$ ) and yield ( $y_2$ ), were evaluated. Twenty experimental runs were performed as suggested by the software. The variables and their range were selected based on preliminary studies. Independent variable ranges studied were: temperature (80 to 150 °C), time (2 to 4 h), and  $\text{FeCl}_3$  concentration (0.4 to 0.6 M), while HCl concentration was kept constant at 3 M for all of the experimental runs. Nevertheless, experimental runs were randomized to reduce the effects of residual errors. At the center point, six experiments were conducted under identical conditions to calculate repeatability of the data (Meyers and Montgomery 2002; Montgomery 2008). The complete design matrix depicting the levels of preferred variables is illustrated by Tables 2 and 3. The regression equation was developed based on the basic design matrix proposed by Tables 2 and 3.

### *Statistical analysis*

Experimental data were fitted for regression analysis and to determine the regression coefficients. Statistical significance of the developed models was obtained by the analysis of variance (ANOVA) test. Process parameters were optimized to get a comprehensive region where the responses under consideration would be at a maximum. The performance of the response surface was investigated by using the regression polynomial equation. The generalized polynomial model proposed can be expressed as,

$$Y_i = \beta_0 + \beta_1 x_1 + \beta_2 x_2 + \beta_3 x_3 + \beta_{11} x_1^2 + \beta_{22} x_2^2 + \beta_{33} x_3^2 + \beta_{12} x_1 x_2 + \beta_{13} x_1 x_3 + \beta_{23} x_2 x_3 \quad (2)$$

where  $Y_i$  is the desired response,  $\beta_0$  is the constant term,  $\beta_1, \beta_2$ , and  $\beta_3$  are the regression coefficients for linear effect terms,  $\beta_{11}, \beta_{22}$ , and  $\beta_{33}$  are quadratic effects, and  $\beta_{12}, \beta_{13}$ , and  $\beta_{23}$  are interaction effects. In this model,  $x_1, x_2$ , and  $x_3$  are the process variables.

The ANOVA analysis of the experimental runs provided the regression coefficients for linear, quadratic, and interaction terms individually. The significance of each term for the responses was also evaluated by observing the F-ratio where the probability (p) is less than 0.05. The adequacy of the models was determined using model analysis, the lack-of-fit test, and coefficient of determination ( $R^2$ ) analysis. The experimental design matrix, data analysis, and optimization procedure were carried out using the software Design-Expert version 7.0.0 (Stat-Ease, Inc., USA)

#### Optimization process

The numerical optimization procedure was performed for percentage crystallinity ( $y_1$ ) and yield ( $y_2$ ). The software gave the optimal levels of three factors ( $x_1, x_2$ , and  $x_3$ ) to obtain the highest crystallinity percentage with maximum yield. The goal for each variable was kept within the studied range. Furthermore, a graphical technique in terms of contour plots with 3D response surfaces was used to visualize the relationship between the responses and experimental levels of each variable where one variable was kept constant at the center point and other two variables were varied within the experimental range.

#### Verification of developed models

The adequacy of the developed models for the responses was verified by conducting experiments under the optimum conditions suggested by the software. The experimental and predicted values of the responses were compared and percentage error was calculated in order to check the validity of predicted models.

#### Characterization

The surface morphology of the starting material (PTC) and obtained hydrolyzed PTC was checked by scanning electron microscopy (FEI Quanta 200F) under optimum conditions. The surface functional groups of native PTC and pretreated PTC were detected by Fourier transform infrared (FTIR) spectroscopy (FTIR-Bruker IFS 66/S; Germany). The spectra were recorded from 4000 to 400  $\text{cm}^{-1}$ . The crystalline structure of the samples was analyzed with a Cu-K $\alpha$  radiation source by X-ray diffraction (XRD) (Bruker AXS D8 Advance). The percentage crystallinity was calculated according to Eq. (3) (Terinte *et al.* 2011),

$$C = \frac{I_{002} - I_{am}}{I_{002}} \times 100 \quad (3)$$

where  $C$  is the percentage crystallinity,  $I_{002}$  is the maximum intensity of the 002 peak at  $2\theta = 22.50$ , and  $I_{am}$  is the intensity at  $2\theta = 18.70$ . Proximate analysis was carried out using thermal gravimetric analysis (TGA) equipment (Mettler Toledo TGA/SDTA 851 $^\circ$ ) to observe the weight loss of the native PTC and hydrolyzed PTC sample under optimum conditions.

## RESULTS AND DISCUSSION

### Development of Mathematical Model and Interpretation of Regression Analysis

The models depicting percentage crystallinity ( $y_1$ ) and yield ( $y_2$ ) for hydrolyzed palm tree cellulose (PTC) were developed based on the highest order polynomials. The additional terms are significant and the models were not aliased based on the sequential model sum of squares (Arami-Niya *et al.* 2011; Chowdhury *et al.* 2012). The parameters describing the reaction conditions in terms of actual and coded factors for model development were calculated from the basic design matrix of Table 2 and Table 3.

**Table 2.** Independent Variables for Acid Hydrolysis with their Actual and Coded Levels

Variables	Code	Units	Coded Variable Levels				
			$-\alpha$	-1	0	+1	$+\alpha$
Temperature	$x_1$	°C	56.14	80	115	150	173.86
Hydrolysis Time	$x_2$	Hour	1.32	2	3	4	4.68
Catalyst FeCl <sub>3</sub> concentration	$x_3$	M	0.26	0.4	1.5	0.8	0.92

The independent variables are coded as (-1, +1) interval where the low and high levels are represented by -1 and +1, respectively. The axial points are denoted as (0, 0,  $\pm\alpha$ ), (0,  $\pm\alpha$ , 0), and ( $\pm\alpha$ , 0, 0). Here,  $\alpha$  indicates the distance between axial points with the center. The complete experimental matrix shown by Table 2 is composed of 6 axial points, 8 factorial points, and 6 center points where the experiments are conducted in identical conditions to determine the residual error.

For crystallinity percentage ( $y_1$ ) and yield ( $y_2$ ), quadratic models were developed. Equations (4) and (5) represent the final empirical equations expressed using the coded factors:

$$\text{Crystallinity Percentage } y_1 = +62.43 + 10.21x_1 + 3.75x_2 + 3.22x_3 + 0.40x_1x_2 + 0.15x_2x_3 - 0.90x_3x_1 + 2.44x_1^2 + 2.52x_2^2 + 2.95x_3^2 \quad (4)$$

$$\text{Percentage Yield } y_2 = +85.12 - 9.61x_1 - 2.19x_2 - 1.69x_3 - 0.81x_1x_2 - 0.42x_2x_3 - 0.70x_1x_3 - 2.53x_1^2 - 1.13x_2^2 - 1.66x_3^2 \quad (5)$$

The linear coefficients for the reaction variables of temperature ( $x_1$ ), time ( $x_2$ ), and catalyst concentration ( $x_3$ ) show the effect of that individual factor for hydrolysis of PTC. On the contrary, the coefficient represented by the product of two factors such as  $x_1x_2$ ,  $x_2x_3$ , and  $x_3x_1$  illustrates the interaction effects on the responses. Second-order terms related to  $x_1^2$ ,  $x_2^2$  and  $x_3^2$  represent a quadratic effect. A positive sign indicates a synergistic effect, whereas a negative sign indicates an antagonistic effect (Arami-Niya *et al.* 2011; Chowdhury *et al.* 2012).

**Table 3.** Experimental Design Matrix for Catalytic Acid Hydrolysis of Palm Tree Trunk Cellulosic Fiber (PTC)

Sample ID	Run	Type of Point	Level (coded Factors)			Reaction Variables (Actual Factors)			Percentage Crystallinity $y_1$	Percentage Yield $y_2$
						Temperature $x_1$ (°C)	Time, $x_2$ (h)	Catalyst concentration, $x_3$ (M)		
S-1	1	Fact	-1	-1	-1	80.00	2.00	0.40	53.99	92.8
S-2	2	Fact	+1	-1	-1	150.00	2.00	0.40	76.99	73.9
S-3	3	Fact	-1	+1	-1	80.00	4.00	0.40	55.69	92.00
S-4	4	Fact	+1	+1	-1	150.00	4.00	0.80	85.88	63.0
S-5	5	Fact	-1	-1	+1	80.00	2.00	0.80	60.78	90.5
S-6	6	Fact	+1	-1	+1	150.00	2.00	0.80	80.99	68.8
S-7	7	Fact	-1	+1	+1	80.00	4.00	0.80	64.89	88.0
S-8	8	Fact	+1	+1	+1	150.00	4.00	0.80	85.88	63.0
S-9	9	Axial	-1.681	0	0	56.14	3.00	0.60	54.89	90.8
S-10	10	Axial	+1.681	0	0	173.86	3.00	0.60	83.88	65
S-11	11	Axial	0	-1.681	0	115.00	1.32	0.60	58.76	86.8
S-12	12	Axial	0	+1.681	0	115.00	4.68	0.60	80.45	76.9
S-13	13	Axial	0	0	-1.681	115.00	3.00	0.26	65.09	81.8
S-14	14	Axial	0	0	+1.681	115.00	3.00	0.94	76.54	78.9
S-15	15	Center	0	0	0	115.00	3.00	0.60	61.68	85.9
S-16	16	Center	0	0	0	115.00	3.00	0.60	62.77	84.9
S-17	17	Center	0	0	0	115.00	3.00	0.60	63.55	84.01
S-18	18	Center	0	0	0	115.00	3.00	0.60	60.99	85.44
S-19	19	Center	0	0	0	115.00	3.00	0.60	61.99	85.00
S-20	20	Center	0	0	0	115.00	3.00	0.60	63.56	85.5

Figures 1a and 1b show the linear plots of predicted *versus* experimental percentage crystallinity ( $y_1$ ) and yield ( $y_2$ ), respectively. As can be observed from these two plots, the predicted values for percentage crystallinity and MCC yield were fairly close to their experimental values. The  $R^2$  values for equations (4) and (5) were 0.95 and 0.96 for percentage crystallinity (Fig. 1a) and yield (Fig. 1b), respectively.

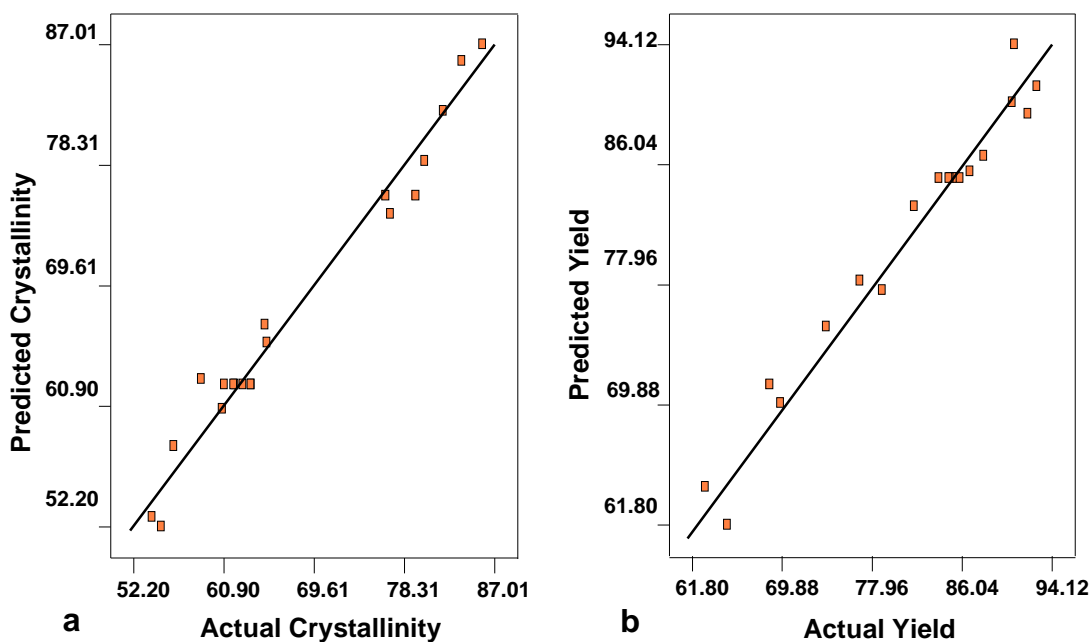


**Fig. 1.** Predicted *versus* actual (a) percentage crystallinity  $y_1$  and (b) percentage yield  $y_2$  of acid hydrolyzed palm tree cellulose (PTC)

### Interpretation of Residual Plots

The normality of the data recorded for each experimental run can be checked by plotting the normal probability plot of the residuals for crystallinity percentage ( $y_1$ ) and yield ( $y_2$ ). The normal probability plot is a graphical representation for evaluating whether or not the data set obtained is approximately normally scattered. Basically, residual shows the difference between the experimental and the fitted or predicted value for model regression. If the data points on the plot are distributed fairly adjacent with the straight line, then it is assumed that the data are normally disseminated. From Fig. 2a and 2b, it is observed that the residual points were aligned with the straight line satisfactorily, signifying normal distribution.

Figures 3a and 3b show Studentized residuals *versus* the fitted value, whereas Figs. 4a and 4b show Studentized residuals *versus* experimental runs for percentage crystallinity ( $y_1$ ) and percentage yield ( $y_2$ ), respectively. The data points for residuals are randomly scattered about zero. This reveals that the variance of experimental observations is constant. All of the data points observed are found to fall within the range of +3 to -3. This ensures that no response transformation is necessary for the experimental design of this study.

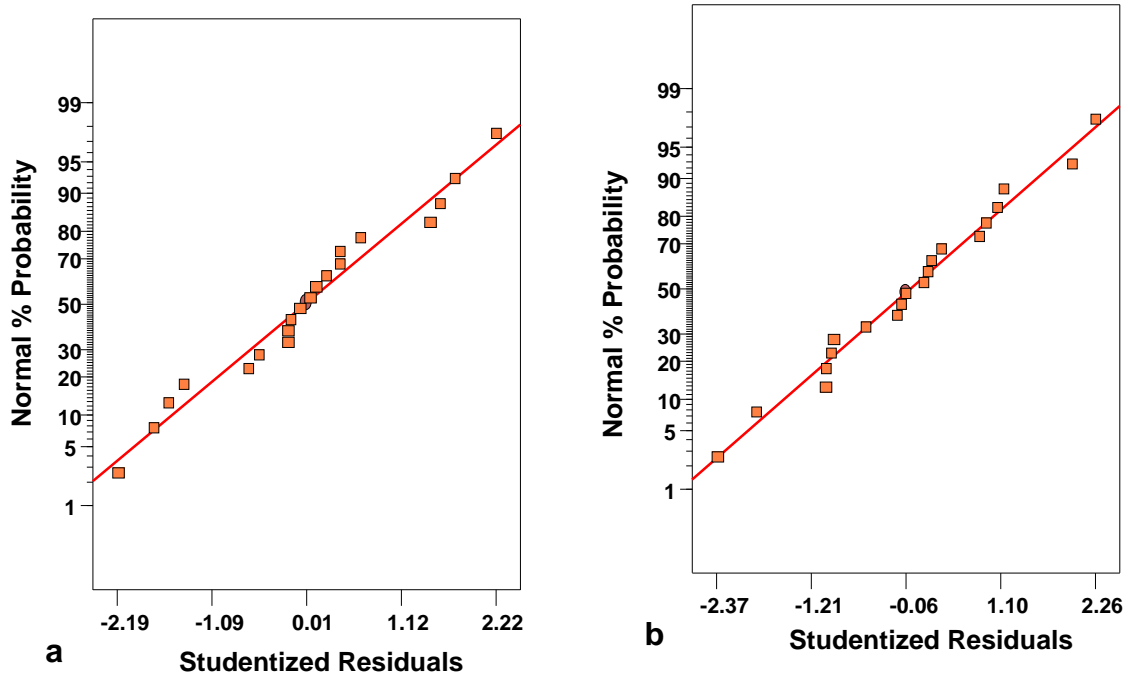


Fig. 2. Normal probability plot residuals (a) percentage crystallinity ( $y_1$ ) and (b) percentage yield ( $y_2$ ) of acid hydrolyzed palm tree cellulose (PTC)

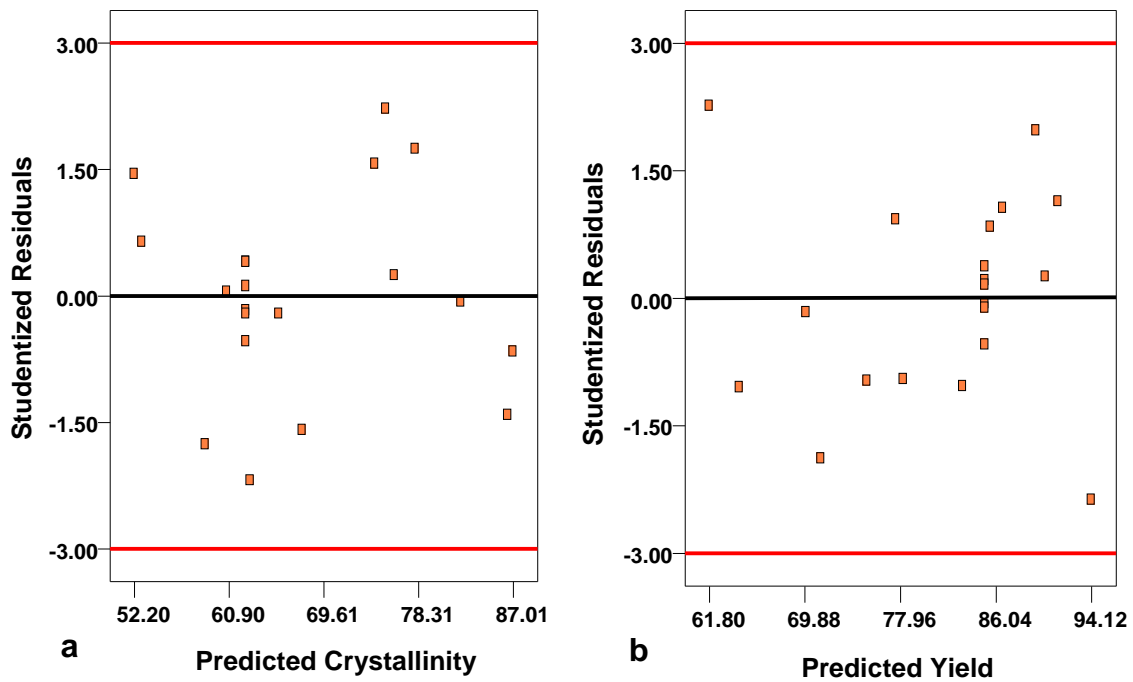
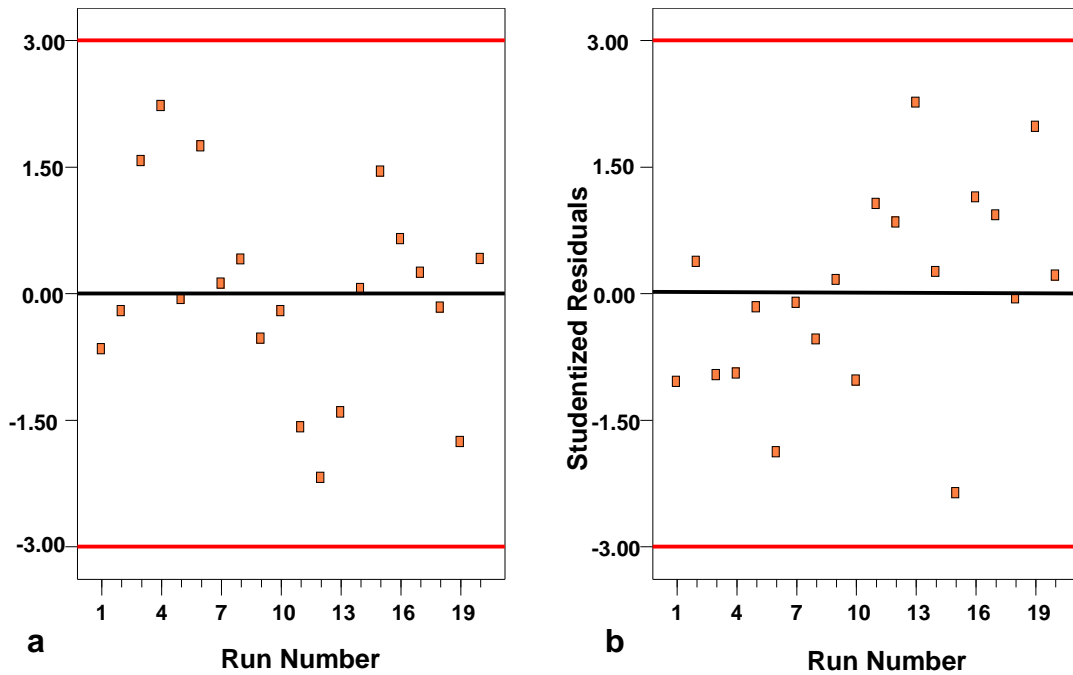
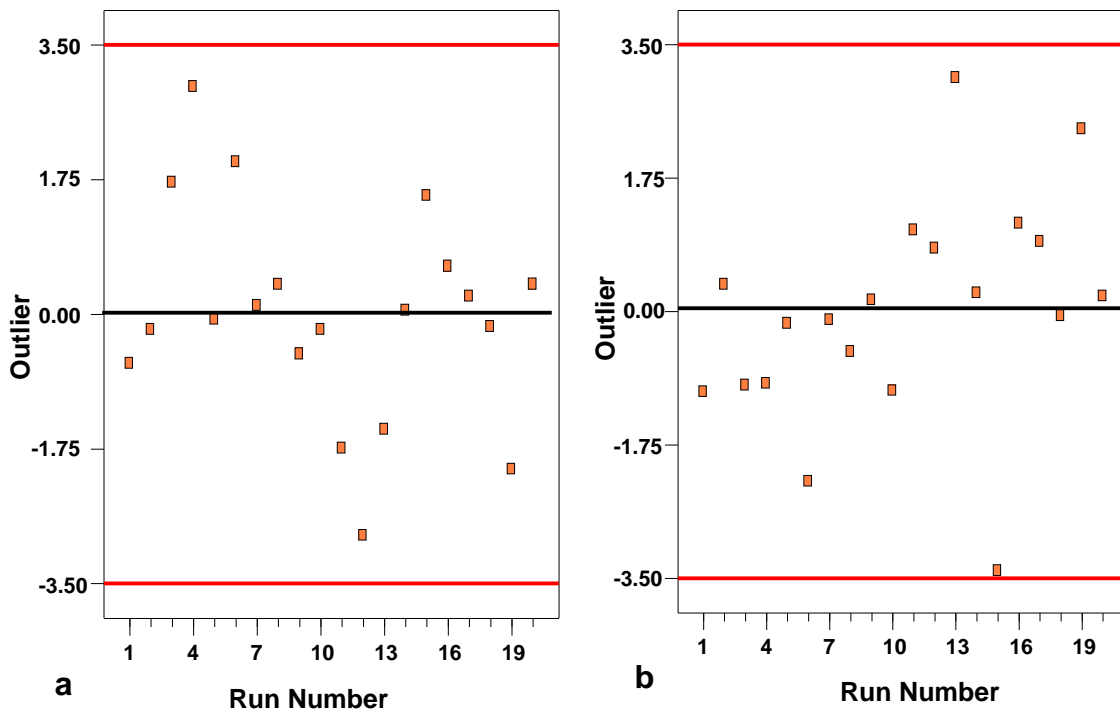


Fig. 3. Studentized residuals versus fitted plot (a) percentage crystallinity ( $y_1$ ) and (b) percentage yield ( $y_2$ ) of acid hydrolyzed palm tree cellulose (PTC)



**Fig. 4.** Studentized residuals *versus* run number (a) percentage crystallinity ( $y_1$ ) and (b) percentage yield ( $y_2$ ) of acid hydrolyzed palm tree cellulose (PTC)

The outlier t-plots for percentage crystallinity ( $y_1$ ) and yield ( $y_2$ ) are illustrated by Figs. 5a and 5b.



**Fig. 5.** Outlier t plot for (a) percentage crystallinity ( $y_1$ ) and (b) percentage yield ( $y_2$ ) of acid hydrolyzed palm tree cellulose (PTC)

Data recording errors were analyzed by observing the t-plots. Nevertheless, outlier t-plots provide sufficient information about the region of independent variables where the fitted model has shown poor approximation to the true response surfaces (Chowdhury *et al.* 2012). It can be seen from Figs. 5a and 5b that most of the standard residuals fell within the interval range of  $\pm 3.50$ . This further ensures that the data approximation for the developed models (Eqs. 1 and 2) to the response surface is fairly good exhibiting no data recording error.

### ANOVA Analysis and Lack of Fit

The experimental results obtained are analyzed by analysis of variance (ANOVA) to measure the precision of the model. The statistical significance of the ratio of mean square variation and mean square residual error were verified using ANOVA. The regression coefficients of the models, corresponding  $R^2$  values, and lack of fit tests are provided in Table 4. The quality of the models can be further verified by the standard deviation. From Table 4, it was observed that experimental  $R^2$  values were in reasonable agreement with the adjusted  $R^2$ . Moreover, the small values of co-efficient of variation (CV) as well as standard deviation reflect reproducibility of the model. The signal to noise ratio was determined in terms of adequate precision. For effective determination of the model, this value should be larger than 4. The adequate precision obtained for crystallinity ( $y_1$ ) and yield ( $y_2$ ) are 16.52 and 20.28, respectively. This further suggests that the developed models could be used to navigate the design.

**Table 4.** Statistical Parameters for ANOVA Analysis for Model Regression for Percentage Crystallinity ( $y_1$ ) and Yield ( $y_2$ )

Statistical Parameters	% Crystallinity	% Yield
	$y_1$	$y_2$
Standard Deviation (SD%)	3.28	2.25
Correlation Coefficient ( $R^2$ )	0.95	0.97
Adjusted $R^2$	0.91	0.94
Mean	67.73	81.48
Coefficient of Variation (CV)	4.40	2.76
Adeq. Precision	16.52	20.28

The significance of linear, interaction, and quadratic model terms were determined using the F-test and p-value as presented in Tables 5 and 6. The most significant variable influencing the percentage crystallinity and yield was the linear term of temperature ( $x_1$ ). The results demonstrated that the regression models for the responses of yield and crystallinity percentage are significant by the F-test at the 5% confidence level.

The  $R^2$  values for these response variables were higher than 0.80 (0.95 to 0.97), which ensures satisfactory fitness of the regression models with the experimental data. In addition, the F-test was carried out to define the process that has a significant effect on both the responses. Generally, the alteration of the process parameter has a substantial effect on the quality characteristics when F is large. The results of ANOVA designated that the considered process parameters were highly significant factors affecting crystallinity

percentage ( $y_1$ ) and yield ( $y_2$ ) of MCC. The value of probable F was less than 0.0001 for percentage crystallinity ( $y_1$ ) and yield ( $y_2$ ), reflecting the significance of the model.

**Table 5.** ANOVA Analysis and Lack of Fit Test for Response Surface Model for Percentage Crystallinity ( $y_1$ )

Source	Sum of Squares	Degree of Freedom	Mean Square	F Value	Prob > F	Comments
Model	1998.72	9	222.08	25.02	< 0.0001	<i>Significant</i>
$x_1$	1421.99	1	1421.99	160.21	< 0.0001	
$x_2$	187.45	1	187.45	21.12	0.0010	
$x_3$	135.62	1	135.62	15.28	0.0029	
$x_1^2$	85.74	1	85.74	9.66	0.0111	
$x_2^2$	78.92	1	78.92	8.89	0.0138	
$x_3^3$	124.96	1	124.96	14.08	0.0038	
$x_1x_2$	2.12	1	2.18	0.25	0.6306	
$x_1x_3$	8.40	1	8.40	0.95	0.3534	
$x_2x_3$	0.61	1	0.61	0.068	0.7993	
Residuals	88.76	10	8.88			
Lack of Fit	83.54	5	16.71	16.03	0.0043	<i>Significant</i>
Pure Error	5.21	5	1.04			

**Table 6.** ANOVA Analysis and Lack of Fit Test for Response Surface Model for Percentage Yield ( $y_2$ )

Source	Sum of Squares	Degree of Freedom	Mean Square	F Value	Prob > F	Comments
Model	1505.32	9	167.26	32.96	< 0.0001	<i>Significant</i>
$x_1$	1260.74	1	1260.74	248.44	< 0.0001	
$x_2$	65.43	1	65.43	12.89	0.0049	
$x_3$	38.48	1	38.48	7.58	0.0204	
$x_1^2$	92.29	1	92.29	18.19	0.0017	
$x_2^2$	18.59	1	18.59	3.66	0.0846	
$x_3^3$	39.92	1	39.92	7.87	0.0186	
$x_1x_2$	5.41	1	5.41	1.07	0.3261	
$x_1x_3$	3.98	1	3.98	0.78	0.3968	
$x_2x_3$	1.51	1	1.51	0.30	0.5969	
Residuals	50.75	10	5.07			
Lack of Fit	48.53	5	9.71	21.90	0.0021	<i>Significant</i>
Pure Error	2.22	5	0.44	32.96	< 0.0001	

From Table 5, it can be observed that temperature ( $x_1$ ), pretreatment time ( $x_2$ ), catalyst concentration ( $x_3$ ), and their quadratic terms of ( $x_1^2$ ), ( $x_2^2$ ), and  $x_3^2$  were significant model terms. Referring to Table 6 for the quadratic model of MCC yield,  $x_1$ ,  $x_2$ , and  $x_3$ , as well as the quadratic terms of  $x_1^2$  and  $x_3^2$  were significant model terms, whereas other interaction terms are negligible relative to the response. For percentage crystallinity ( $y_1$ )

and yield ( $y_2$ ), temperature had the greatest effect on these responses by showing the highest F values of 1421.99 and 1260.74, respectively, as shown in Tables 5 and 6. Hydrolyzing time ( $x_2$ ) and catalyst concentration ( $x_3$ ) had moderate effects, whereas the interaction effect of temperature and time ( $x_1x_2$ ) and temperature and catalyst concentration ( $x_1x_3$ ) were more prominent than the other two interaction terms relative to the percentage crystallinity and yield, respectively.

### Process Variables Optimization

When producing microcrystalline cellulose (MCC), relatively high product yields are expected so that further degradation of the crystalline portion of MCC in harsher conditions can be prevented. The most important property of microcrystalline cellulose is its percentage crystallinity. Therefore, in a practical manufacturing process, a compromise should be made between the yield and the percentage crystallinity to ensure selective acid hydrolysis of the amorphous region, as well as to prevent char formation by using comparatively mild conditions. However, optimization of both of these responses under the same condition is difficult because the interest region of the factors is different. As observed from the basic design matrix, when the percentage crystallinity increases, the yield decreases and vice versa. Therefore, in order to achieve a compromise between these two responses, the numerical optimization menu is selected. In order to optimize the preparation conditions, the targeted criteria is set as maximum values for the two responses, while the values of the three variables (temperature, time, and catalyst concentration) are set in the ranges being studied. The sample has been prepared under optimum conditions and the experimental results are compared with the predicted values. The percentage deviation between the predicted and experimental conditions is evaluated and presented in Table 7.

**Table 7.** Process Parameter Optimization for Acid Hydrolysis of MCC in Presence of  $\text{FeCl}_3$

Hydrolysis Temp. (°C)	Hydrolysis Time (Hour)	Catalyst Con. (M)	Percentage Crystallinity ( $y_1$ )			Percentage Yield ( $y_2$ )		
			Predicted	Experimental	Error	Predicted	Experimental	Error
97.98	4	0.8	70.73	68.66	2.92	82.80	83.98	1.42

Under identical conditions of temperature, time, and acid concentration, the reaction was conducted without adding  $\text{FeCl}_3$  catalyst. The prepared sample exhibited a crystallinity index of 58.22%.

### Interpretation of Surface Contour Plots

Figure 6a is constructed to show the three-dimensional response surfaces with a contour plot, which shows the combined effect of two significant variables (temperature and time) on percentage crystallinity ( $y_1$ ) of extracted microcrystalline cellulose (MCC) where the catalyst concentration is kept at the center point, which is the zero level (0.60). Figure 6b shows the combined effect of hydrolysis temperature and catalyst concentration on percentage crystallinity, where the hydrolyzing time is fixed at the zero level, which is 3 h. In this work, the three variables studied were found to have synergistic effects on

percentage crystallinity. Percentage crystallinity was increased significantly when temperature and time were at the maximum (Fig. 6a). This is expected, as the progressive increase of temperature and hydrolyzing time increases the diffusion of hydrochloric acid as well as the catalyst solution inside the cellulosic matrix which would initiate the disintegration of the amorphous region of cellulose. Sufficient contact time also causes physical swelling of PTC, which in turn increases the surface area of the sample. Consequently, hydrolysis efficiency becomes higher. However, prolonged contact time for hydrolyzing is not suggested, as it might decrease the yield with a successive decrease of crystallinity.

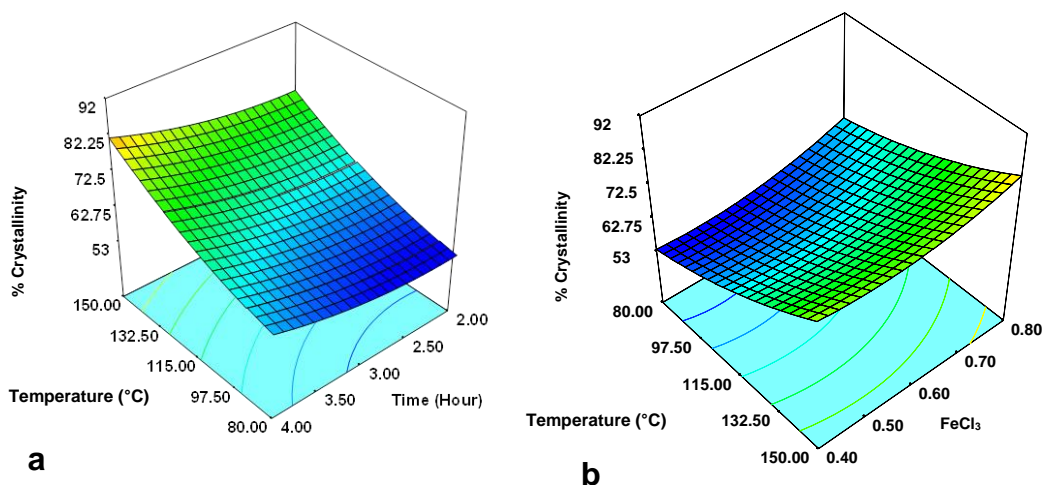
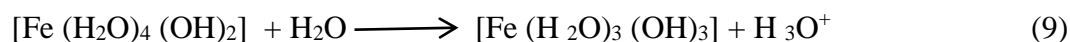
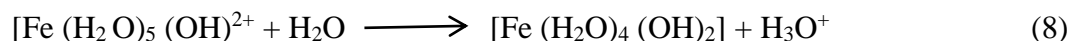


**Fig. 6.** Response surface and contour plots of the combined effects of (a) temperature and time and (b) temperature and catalyst concentration on percentage crystallinity ( $y_1$ ) of acid hydrolyzed MCC when the other two variables are at center points

Increasing the concentration of the metal ion catalyst, which was acting as a Lewis acid, increased the percentage crystallinity ( $y_1$ ). At the initial stage,  $\text{Fe}^{3+}$  forms a coordination complex with water to yield  $\text{H}_3\text{O}^+$  ions.  $\text{Fe}^{3+}$  will form a coordinate covalent bond with 6 water molecules resulting in metal-ligand complexes of  $[\text{M}(\text{H}_2\text{O})_n]^{Z+}$ , where M represents the cation, Z is the oxidation state of the cation, and n is the solvation number, which is between 4 and 6. The reaction scheme is shown by following equations (Li *et al.* 2013):



The central metal ions polarize the water molecules by withdrawing electron density. This makes the hydrogen atoms in O-H bond more electropositive. The complex

ions deprotonate, making the solution acidic. Enhanced acidity due to presence of  $\text{H}_3\text{O}^+$  ions breaks down the glycosidic linkage between the glucose units of cellulose. Oxygen atoms of the glucose unit in cellulose can readily form intermediate complexes by absorbing  $\text{Fe}^{3+}$  ions. This oxygen-iron co-ordination complex increases pyranose bond length and bond angle, resulting in lower activation energy of the reaction. Thus hydrolysis efficiency is greater (Zhao *et al.* 2011). However, as stated earlier, process parameters must be optimized to reduce the formation of char with the production of furfural and 5-hydroxymethylfurfural as secondary products according to the following reaction scheme:

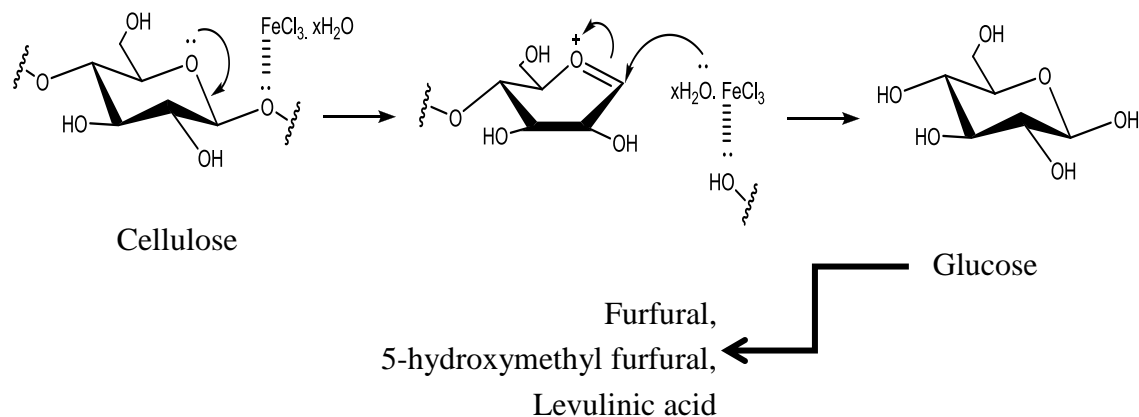


**Fig. 7.** Proposed reaction scheme for catalytic acid hydrolysis of palm tree cellulose (PTC)

Figs 8a and 8b show the 3D response surfaces that are constructed to reveal the effects of reaction variables on MCC yield. Figure 8a represents the combined effect of temperature and time on the response, where the catalyst concentration is fixed at the zero level (0.6 M). Figure 8b illustrates the effect of temperature and catalyst concentration on the same response, where time is fixed at the zero level (3 h).

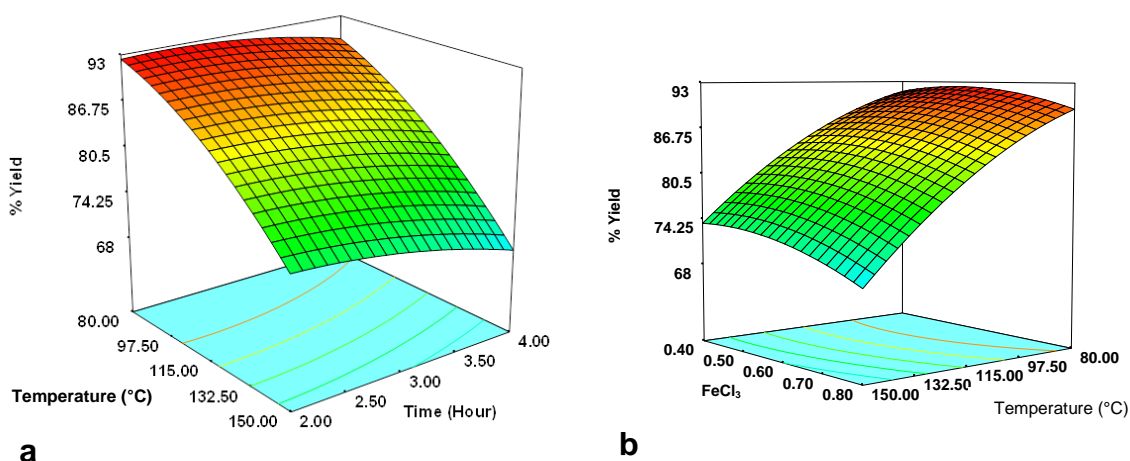


**Fig. 8.** Response surface and contour plots of the combined effects of (a) temperature and time and (b) temperature and catalyst concentration on percentage yield ( $y_2$ ) of acid hydrolyzed MCC when the other two variables are at center points

In general, yield was found to decrease with increased temperature, time, and catalyst concentration. As can be seen from both the plots (Figs. 8a and 8b), temperature was more dominant relative to the yield as compared to the other two variables. The lowest yield was obtained when temperature was at the maximum point (173.86 °C, Sample 10) within the studied range as depicted by the design matrix of Table 2. This is due to chemical degradation of cellulose in acid hydrolyzing medium (Zhao *et al.* 2011).

### Physiochemical Characterization of the Hydrocellulose

The changes in the structures of the treated MCC particles due to acid hydrolysis in the presence of FeCl<sub>3</sub> catalyst were confirmed by the images obtained from scanning electron microscopy (Fig. 9). The morphological changes in the structures of the hydrolyzed palm tree cellulose (PTC) compared to the native cellulose fibers were confirmed by the images obtained from scanning electron microscopy (Fig. 9). The results confirmed obvious size reduction and fractures of the PTC sample treated under optimum conditions.

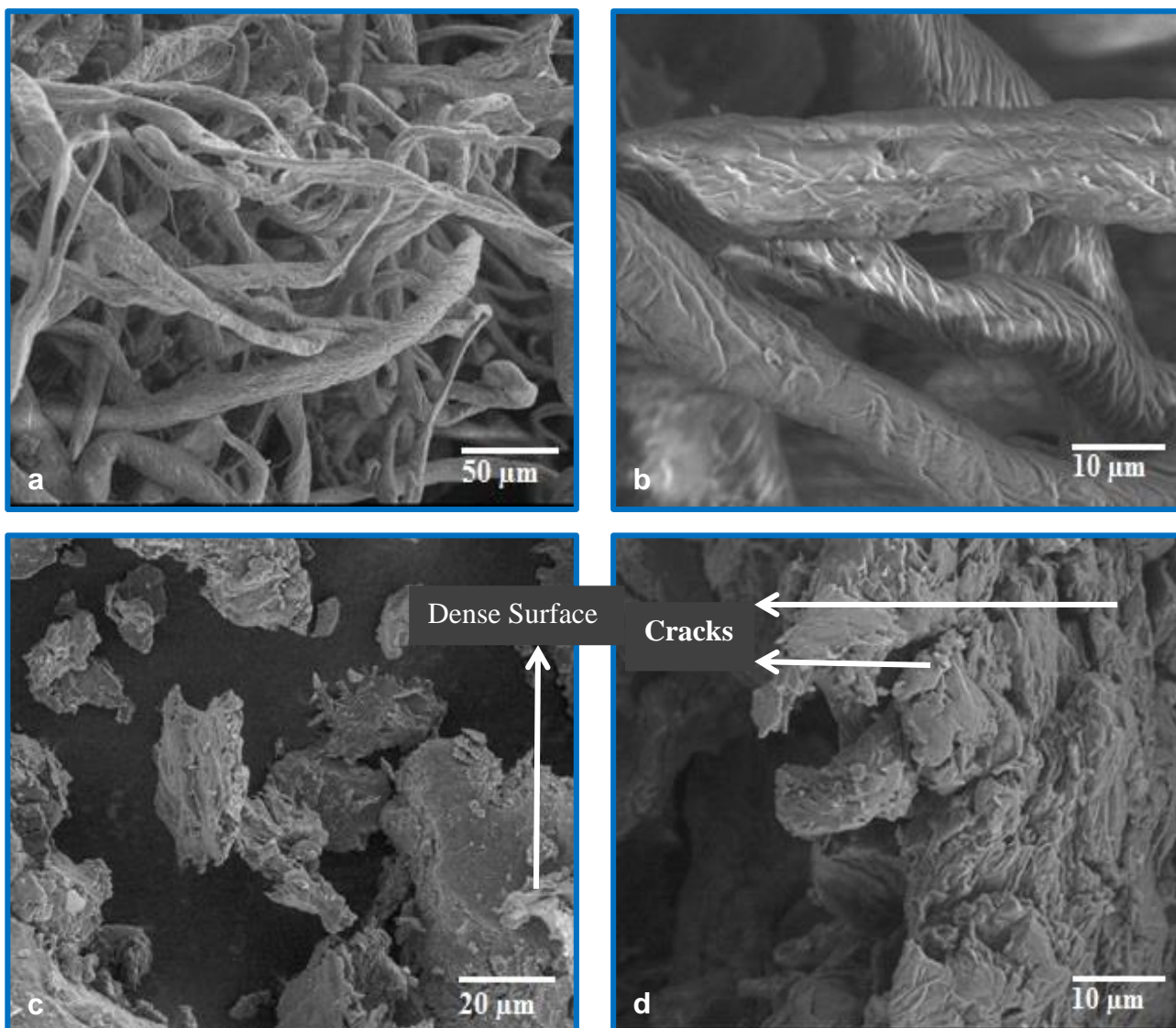
Figure 9a illustrates the structure of native PTC, which is comparatively uniform, flat, and smooth even at lower magnification. This exhibits the rigid and well-ordered structure of cellulose. At higher magnification (Fig. 9b), some folds were observed over the surface of PTC. This type of structural feature of native palm tree cellulose provides adequate contact area for accessibility of FeCl<sub>3</sub> catalyst as well as HCl acid itself (Li *et al.* 2013).

Figure 9c shows images of the sample treated under optimum conditions where the HCl concentration was fixed at 3 M, the catalyst concentration at 0.8 M, hydrolyzing time of 4 h, and hydrolyzing temperature of 97.98 °C. The fibers were degraded into fragments due to chemical swelling and acid hydrolysis. The results are in agreement for acid hydrolysis of waste banana peel fibers (Elanthikkal *et al.* 2010). The end products are agglomerated, which are similar to the MCC particles derived from Norway spruce previously observed by Bondsen *et al.* (2006). Loss of orderly fibrillar structure of treated PTC indicates surface etching coupled with a certain degree of erosion. Comparatively large number of cracks and crevices are visible over the surface of the hydrolyzed PTC (Fig. 9d).

These cracks appeared due to quick diffusion of acid and metal ions inside the cell wall of the fiber. The dense structure visible in Fig. 9d represents the high crystalline region of cellulose. Similar morphological features are reported for catalytic acid hydrolysis of sulfate pulp extracted from hard wood of *Eucalyptus* using FeCl<sub>3</sub> as the catalyst (Li *et al.* 2013; 2014).

### X-ray diffraction

The XRD patterns of the native and hydrolyzed PTC fiber are illustrated in Fig. 10. It was observed previously that the major diffraction peak for cellulose can be observed for 2θ ranging between 22° and 23° as a primary peak, whereas a secondary peak is in the range of 16° to 18° (Li *et al.* 2014).



**Fig. 9.** SEM images of palm tree cellulose (PTC). (a) native PTC fiber, (b) native PTC fiber, (c) hydrolyzed PTC fiber under optimum conditions, and (d) hydrolyzed PTC fiber under optimum conditions

From the XRD distribution pattern, noticeable peaks can be observed within the stated range for both the sample reflecting the typical structure of native cellulose or cellulose I. This indicates that the whole structure of cellulose was not disrupted by catalytic acid hydrolysis under optimum conditions (Li *et al.* 2014). However, the hydrolyzed sample showed a higher peak intensity, which might be due to the partial breaking up of glycoside linkages inside the amorphous region, whereas the well-organized crystalline region was only slightly affected. The percentage crystallinity observed for palm tree cellulose (PTC) and hydrolyzed samples of PTC under optimum conditions was 52.36 % and 68.66% respectively.

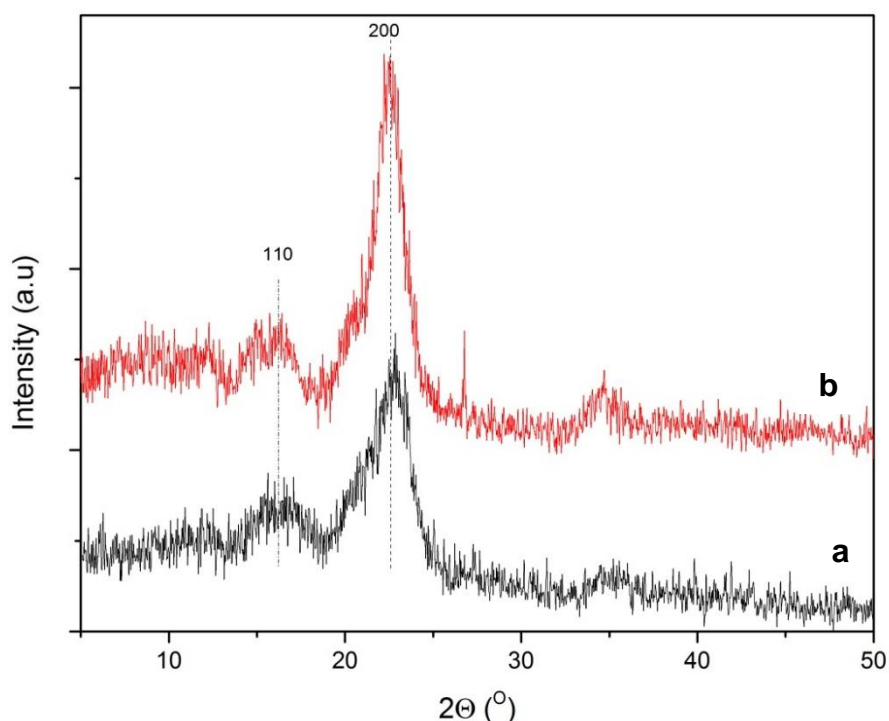


**Fig. 10.** XRD analysis of palm tree cellulose (PTC). (a) native PTC fiber and (b) hydrolyzed PTC fiber under optimum conditions

Thermogravimetric analysis (TGA) and derivative thermogravimetric analysis (DTA) were performed for native PTC and hydrolyzed PTC samples under optimum conditions. The TGA and DTA curves obtained are illustrated in Fig. 11. The thermal degradation data (onset temperature,  $T_{on}$ , 10% weight loss temperature,  $T_{10\%}$ , and 50% weight loss temperature,  $T_{50\%}$ ) along with residual weight loss around 700 °C, including peak degradation temperature, is provided in Table 8.

**Table 8.** Thermogravimetric Analysis of Untreated and Treated MCC

Sample	Degradation Temperature °C			DTG Peak Temperature °C	Residual weight loss at 700 °C
	$T_{on}$	$T_{10\%}$	$T_{50\%}$	$T_{max}$	
Native PTC fiber	195	265	323	320	20.19
Hydrolyzed PTC fiber at optimum conditions	225	295	340	330	18.58

Initial weight loss was observed around 100 to 110 °C. This weight loss was due to evaporation of moisture present in PTC sample. After that, the loss in weight of the cellulosic fiber increased up to a greater extent. The loss in weight percentage was greater for native PTC fiber than for hydrolyzed PTC. This can be attributed to the decrease of disordered amorphous with the increase of hydrogen bonding in the crystalline region of the hydrolyzed sample. Referring to Table 8, it can be observed that the onset temperature,

$T_{on}$ , 10% weight loss temperature,  $T_{10\%}$ , and 50% weight loss temperature,  $T_{50\%}$ , had increased after the catalytic hydrolysis process. Due to acid hydrolysis process in the presence of catalyst, chemical swelling of the sample increased resulting higher crystallinity percentage of hydrolyzed PTC sample.

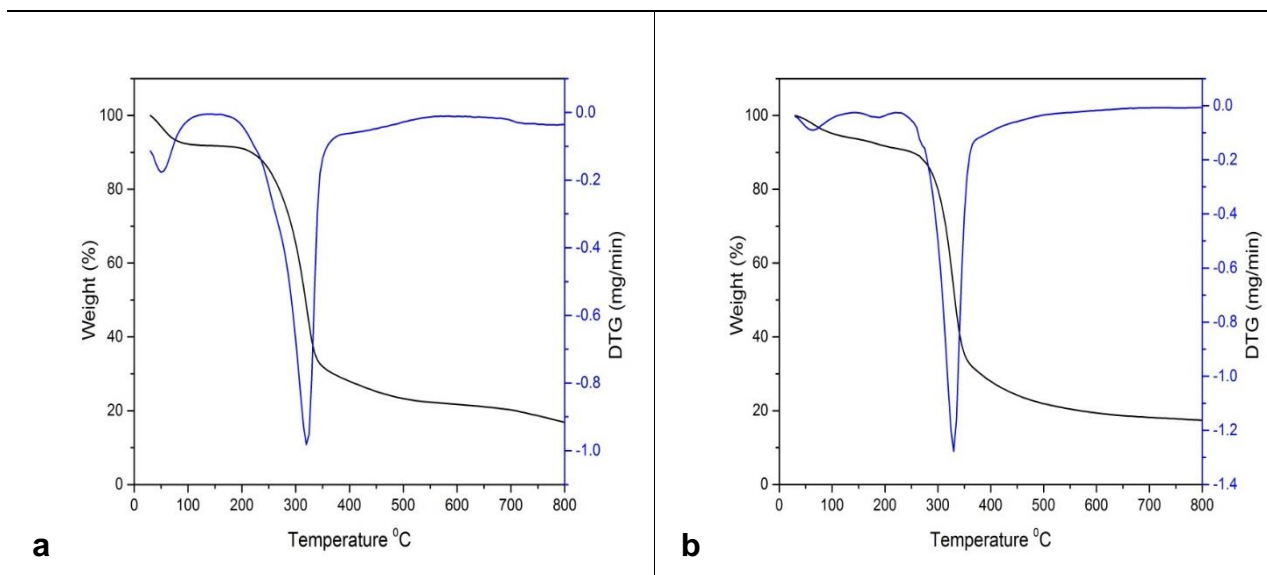


**Fig. 11.** Thermogravimetric analysis of (a) native PTC and (b) hydrolyzed PTC under optimum conditions

The FTIR spectra of the native PTC (Fig. 12a) and hydrolyzed samples (Fig. 12b) are shown in Fig. 12. The FTIR spectra obtained before and after acid swelling in the presence of the catalyst revealed the absence of strong chemical reactions or alteration of major chemical groups. This shows that the treatment cannot completely change the chemical structure of the cellulosic fragments (Chen *et al.* 2010; Mohamad Haafiz *et al.* 2013). The peaks around 3400, 2900, 1400, and 900  $\text{cm}^{-1}$  were present both in untreated and treated samples (Chen *et al.* 2010; Mohamad Haafiz *et al.* 2013). The peaks around 610  $\text{cm}^{-1}$  present in untreated sample changed their frequency level and were observed around 608  $\text{cm}^{-1}$  in the treated sample. The peaks around 898  $\text{cm}^{-1}$  and 897  $\text{cm}^{-1}$  showed a rocking vibration of the  $-\text{C}-\text{H}$  band in cellulose. The band at 1160  $\text{cm}^{-1}$  and 1162  $\text{cm}^{-1}$  ascribed to  $-\text{C}-\text{O}-\text{C}-$  stretching of the  $\beta$ -1, 4-glycosidic linkage was prominent for both native and hydrolyzed PTC samples. The bands at 1424  $\text{cm}^{-1}$  and 1433  $\text{cm}^{-1}$  were endorsed for asymmetric bending and wagging of the  $-\text{CH}_2$  group, for untreated and treated palm tree cellulose (PTC). This shows intermolecular hydrogen attraction at the  $\text{C}_6$  group (Kumar *et al.* 2002). A small, sharp peak around 1640  $\text{cm}^{-1}$  in untreated sample and 1644  $\text{cm}^{-1}$  in treated sample were identified due to absorption of water (Johar *et al.* 2012). The peak around 1564  $\text{cm}^{-1}$  indicates the presence of  $\text{C}=\text{C}$  in plane symmetrical stretching vibration of aromatic ring present for lignin content in untreated PTC sample (Mandal and Chakrabarti 2011). However after hydrolysis, this peak disappeared completely. The peak around 2903  $\text{cm}^{-1}$  and 2905  $\text{cm}^{-1}$  indicate characteristics  $-\text{CH}$  stretching vibration in treated and hydrolyzed sample. The peaks around 3351  $\text{cm}^{-1}$  and 3355  $\text{cm}^{-1}$  indicate  $-\text{OH}$  vibration in both the sample.

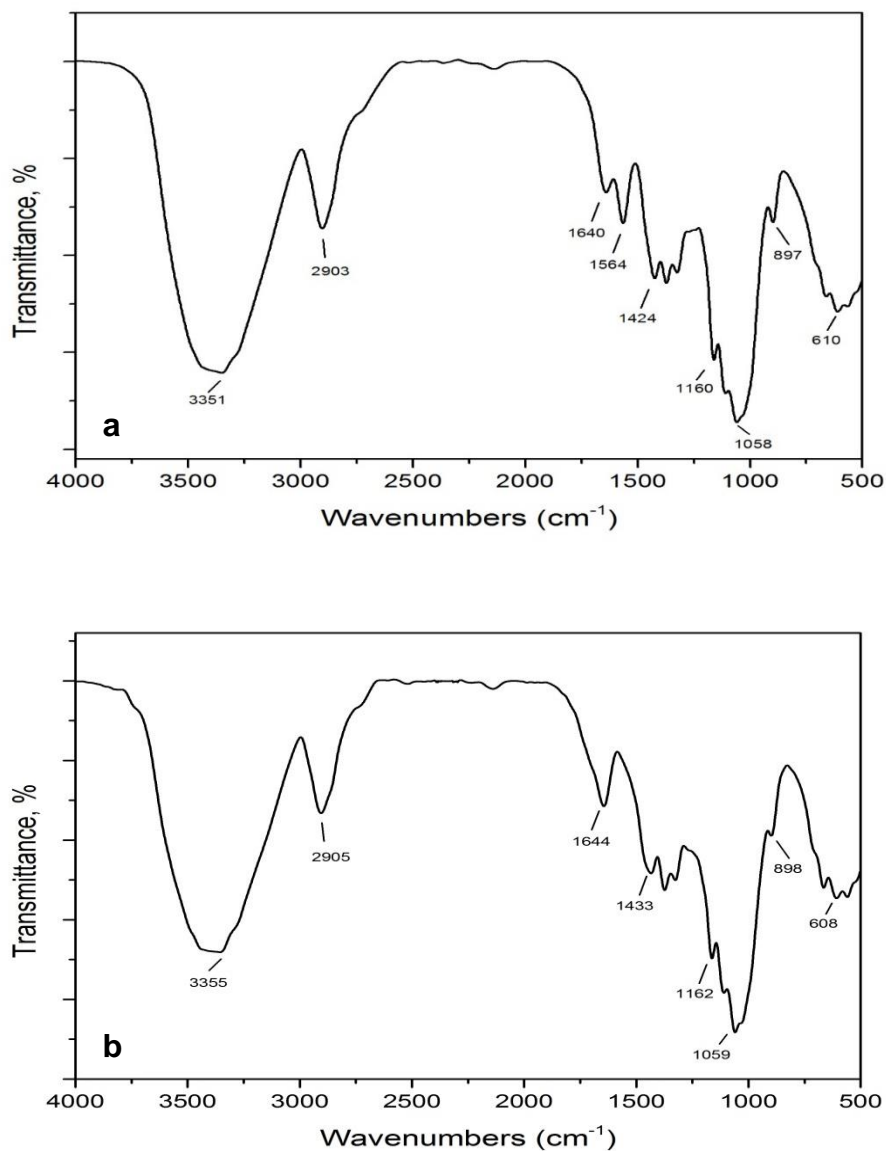


**Fig. 12.** Palm tree cellulose (PTC). (a) native PTC and (b) hydrolyzed PTC sample in the presence of FeCl<sub>3</sub> catalyst

## CONCLUSIONS

1. This study showed successful application of response surface methodology (RSM) in order to establish predictive models for percentage crystallinity ( $y_1$ ) and yield ( $y_2$ ) to produce MCC from palm tree cellulose (PTC).
2. The synergistic effect of FeCl<sub>3</sub> and HCl significantly affected the hydrolysis of the amorphous regions of the cellulosic chain up to a greater extent, but the yield dropped significantly under some harsh conditions of high temperature,

time, and catalyst concentration. Disintegration of the amorphous region during hydrolysis is probably the explanation for poor yield.

3. All three variables of temperature, time, and catalyst concentration were very influential. An apparent interaction effect was observed between hydrolysis temperature and time as well as hydrolysis temperature with catalyst concentration for both of the responses.
4. The factors affecting the percentage crystallinity ( $y_1$ ) and yield ( $y_2$ ) were in the order of: temperature > time > catalyst concentration. Model simulation and theoretical optimization were carried out.
5. The theoretical values for percentage crystallinity and yield were close to experimental values, resulting in a small error percentage of 2.98% and 1.42%, respectively.
6. Microcrystalline cellulose produced under optimum conditions can be used for pharmaceutical products where it is mainly incorporated as an excipient. However, optimum conditions for extracting MCC particles would obviously be different if the starting cellulosic substrate is obtained from other biomass sources.

## ACKNOWLEDGEMENTS

The authors would like to thank High Impact Research (HIR F-000032) for their financial support in this work.

## REFERENCES CITED

- Abdul Khalil, H., Bhat, A., and Ireana Yusra, A. (2012). "Green composites from sustainable cellulose nanofibrils: A review," *Carbohydrate Polymers* 87(2), 963-979. DOI: 10.1016/j.carbpol.2011.08.078
- Adel, A. M., Abd El-Wahab, Z. H., Ibrahim, A. A., and Al-Shemy, M. T. (2011). "Characterization of microcrystalline cellulose prepared from lignocellulosic materials. Part II: Physicochemical properties," *Carbohydrate Polymers* 83(2), 676-687. DOI: 10.1016/j.carbpol.2010.08.039
- Akmar, P., and Kennedy, J. (2001). "The potential of oil and sago palm trunk wastes as carbohydrate resources," *Wood Science and Technology* 35(5), 467-473. DOI: 10.1007/s002260100107
- Arami-Niya, A., Abnisa, F., Sahfeeyan, M. S., Daud, W. W., and Sahu, J. N. (2011). "Optimization of synthesis and characterization of palm shell-based bio-char as a by-product of bio-oil production process," *BioResources* 7(1), 246-264. DOI: 10.15376/biores.7.1.0246-0264
- Azubuiké, C. P., Odulaja, J. O., and Okhamafe, A. O. (2012). "Physicochemical, spectroscopic and thermal properties of powdered cellulose and microcrystalline

- cellulose derived from groundnut shells," *Journal of Excipients and Food Chemicals* 3(3), 106-115.
- Bondeson, D., Mathew, A., and Oksman, K. (2006). "Optimization of the isolation of nanocrystals from microcrystalline cellulose by acid hydrolysis," *Cellulose* 13(2), 171-180. DOI: 10.1007/s10570-006-9061-4
- Chen, W. H., Tu, Y. J., and Sheen, H. K. (2010). "Impact of dilute acid pretreatment on the structure of bagasse for bioethanol production," *International Journal of Energy Research* 34(3), 265-274. DOI: 10.1002/Er.1566
- Chowdhury, Z., Zain, S., Khan, R., Ahmad, A., Islam, M., and Arami-Niya, A. (2011). "Application of central composite design for preparation of Kenaf fiber based activated carbon for adsorption of manganese (II) ion," *International Journal of Physical Sciences* 6(31), 7191-7202. DOI: 10.5897/IJPS11.1510
- Chowdhury, Z. Z., Zain, S. M., Hamid, S. B. A., and Khalid, K. (2014). "Catalytic role of ionic liquids for dissolution and degradation of biomacromolecules," *BioResources* 9(1), 1787-1823. DOI: 10.15376/biores.9.1.1787-1823
- Chowdhury, Z. Z., Zain, S. M., Khan, R. A., Arami-Niya, A., and Khalid, K. (2012). "Process variables optimization for preparation and characterization of novel adsorbent from lignocellulosic waste," *BioResources* 7(3), 3732-3754. DOI: 10.15376/biores.7.3.3732-3754
- Costa, S., Moris, V., and Rocha, S. (2011). "Influence of process variables on granulation of microcrystalline cellulose in vibrofluidized bed," *Powder Technology* 207(1), 454-460. DOI: 10.1016/j.powtec.2010.11.037
- de Mesquita, J. P., Donnici, C. L., and Pereira, F. V. (2010). "Biobased nanocomposites from layer-by-layer assembly of cellulose nanowhiskers with chitosan," *Biomacromolecules* 11(2), 473-480. DOI: 10.1021/bm9011985
- Dungani, R., Jawaid, M., Khalil, H. A., Jasni, J., Aprilia, S., Hakeem, K. R., Hartati, S., and Islam, M. (2013). "A review on quality enhancement of oil palm trunk waste by resin impregnation: Future materials," *BioResources* 8(2), 3136-3156. DOI: 10.15376/biores.8.2.3136-3156
- Ejikeme, P. M. (2008). "Investigation of the physicochemical properties of microcrystalline cellulose from agricultural wastes I: Orange mesocarp," *Cellulose* 15(1), 141-147. DOI: 10.1007/s10570-007-9147-7
- Elanthikkal, S., Gopalakrishnanpanicker, U., Varghese, S., and Guthrie, J. T. (2010). "Cellulose microfibrils produced from banana plant wastes: Isolation and characterization," *Carbohydrate Polymers* 80(3), 852-859. DOI: 10.1016/j.carbpol.2009.12.043
- Follain, N., Marais, M.-F., Montanari, S., and Vignon, M. R. (2010). "Coupling onto surface carboxylated cellulose nanocrystals," *Polymer* 51(23), 5332-5344. DOI: 10.1016/j.polymer.2010.09.001
- Habibi, Y., Lucia, L. A., and Rojas, O. J. (2010). "Cellulose nanocrystals: Chemistry, self-assembly, and applications," *Chemical reviews* 110(6), 3479-3500. DOI: 10.1021/cr900339w
- Hanna, M., Biby, G., and Miladinov, V. (2001). "Production of microcrystalline cellulose by reactive extrusion," *United States Patent Number* 6,228,213.

- Hashaikeh, R., and Abushammala, H. (2011). "Acid mediated networked cellulose: Preparation and characterization," *Carbohydrate Polymers* 83(3), 1088-1094. DOI: 10.1016/j.carbpol.2010.08.081
- Jain, J., Dixit, V., and Varma, K. (1983). "Preparation of microcrystalline cellulose from cereal straw and its evaluation as a tablet excipient," *Indian Journal of Pharmaceutical Science* 45(3), 83-85.
- Johar, N., Ahmad, I., and Dufresne, A. (2012). "Extraction, preparation and characterization of cellulose fibres and nanocrystals from rice husk," *Industrial Crops and Products* 37(1), 93-99. DOI: 10.1016/j.indcrop.2011.12.016
- Kamireddy, S. R., Li, J., Tucker, M., Degenstein, J., and Ji, Y. (2013). "Effects and mechanism of metal chloride salts on pretreatment and enzymatic digestibility of corn stover," *Industrial & Engineering Chemistry Research* 52(5), 1775-1782. DOI: 10.1021/Ie3019609
- Khalil, H., Aprilia, N., Bhat, A., Jawaid, M., Paridah, M., and Rudi, D. (2013). "A *Jatropha* biomass as renewable materials for biocomposites and its applications," *Renewable and Sustainable Energy Reviews* 22, 667-685. DOI: 10.1016/j.rser.2012.12.036
- Kumar, V., de la Luz Reus-Medina, M., and Yang, D. (2002). "Preparation, characterization, and tableting properties of a new cellulose-based pharmaceutical aid," *International Journal of Pharmaceutics* 235(1), 129-140. DOI: 10.1016/S0378-5173(01)00995-4
- Landin, M., Martinez-Pacheco, R., Gomez-Amoza, J., Souto, C., Concheiro, A., and Rowe, R. (1993). "Effect of batch variation and source of pulp on the properties of microcrystalline cellulose," *International Journal of Pharmaceutics* 91(2), 133-141. DOI: 10.1016/0378-5173(93)90332-A
- Li, J., Xiu, H., Zhang, M., Wang, H., Ren, Y., and Ji, Y. (2013). "Enhancement of cellulose acid hydrolysis selectivity using metal ion catalysts," *Current Organic Chemistry* 17(15), 1617-1623.
- Li, J., Zhang, X., Zhang, M., Xiu, H., and He, H. (2014). "Optimization of selective acid hydrolysis of cellulose for microcrystalline cellulose using FeCl<sub>3</sub>," *BioResources* 9(1), 1334-1345. DOI: 10.15376/biores.9.1.1334-1345
- Mandal, A., and Chakrabarty, D. (2011). "Isolation of nanocellulose from waste sugarcane bagasse (SCB) and its characterization," *Carbohydrate Polymers* 86(3), 1291-1299. DOI: 10.1016/j.carbpol.2011.06.030
- Meyers, R. H., and Montgomery, D. C. (2002). *Response Surface Methodology*, Wiley, New York NY.
- Mohamad Haafiz, M., Eichhorn, S., Hassan, A., and Jawaid, M. (2013). "Isolation and characterization of microcrystalline cellulose from oil palm biomass residue," *Carbohydrate Polymers* 93(2), 628-634. DOI: 10.1016/j.carbpol.2013.01.035
- Montgomery, D. C. (2008). *Design and Analysis of Experiments*, John Wiley & Sons, New York.
- Moon, R. J., Martini, A., Nairn, J., Simonsen, J., and Youngblood, J. (2011). "Cellulose nanomaterials review: Structure, properties and nanocomposites," *Chemical Society Reviews* 40(7), 3941-3994. DOI: 10.1039/c0cs00108b
- Nada, A.-A. M., El-Kady, M. Y., El-Sayed, E. S. A., and Amine, F. M. (2009). "Preparation and characterization of microcrystalline cellulose (MCC),"

- BioResources* 4(4), 1359-1371. DOI: 10.15376/biores.4.4.1359-1371
- Nguyen, Q. A., and Tucker, M. P. (2002). "Dilute acid/metal salt hydrolysis of lignocellulosics," *United States Patent*, Number 6,423,145.
- Ofoefule, S., and Chukwu, A. (1999). "Application of blends of MCC- Cissus gum in the formation of aqueous suspensions," *Bollettino Chim. Farmaceutico* 138(5), 217-222.
- Ohwoavworhwa, F., Kunle, O., and Ofoefule, S. (2004). "Extraction and characterization of microcrystalline cellulose derived from *Luffa cylindrica* plant," *African Journal of Pharmaceutical Research & Development* 1(1), 1-6.
- Okhamafe, A., and Azubuikwe, C. (1994). "Direct compression studies on low-cost cellulose derived from maize cob," *Journal of Pharmaceutical Sciences and Pharmacy Practice* 2, 26-29.
- Okhamafe, A., Ejike, E., Akinrinola, F., and Ubane-Ine, D. (1995). "Aspect of tablet disintegrant properties of cellulose derived from bagasse and maize cob," *West African Journal of Pharmacy* 9(1), 8-13.
- Okhamafe, A., Igboechi, A., and Obaseki, T. (1991). "Celluloses extracted from groundnut shell and rice husk 1: Preliminary physicochemical characterization," *Pharmacy World Journal* 8(4), 120-130.
- Omray, A., and Omray, P. (1986). "Evaluation of microcrystalline cellulose as a glidant," *Indian Journal of Pharmaceutical Science* 48, 20-22.
- Proenca, H. A. G. (1999). "Process for rapid acid hydrolysis of lignocellulosic material and hydrolysis reactor," *United States Patent*, Number 5,879,463.
- Ren, L.-b., Cao, Q., and Xie, X.-l. (2012). "Hydrolysis kinetics of microcrystalline cellulose catalyzed by Fe<sup>3+</sup> and dilute hydrochloric acid," *Chemistry and Industry of Forest Products* 32(4), 117-122.
- Rowe, R. C., Sheskey, P. J., and Owen, S. C. (2006). *Handbook of Pharmaceutical Excipients*, Pharmaceutical Press, London.
- Saleh, T. M., and El-Ashmawy, A. E. (1978). "Alkaline pulping of mixed reed and bagasse," *Journal of Chemical Technology and Biotechnology* 28(11), 721-726. DOI: 10.1002/jctb.5700281105
- Sulaiman, O., Salim, N., Nordin, N. A., Hashim, R., Ibrahim, M., and Sato, M. (2012). "The potential of oil palm trunk biomass as an alternative source for compressed wood," *BioResources* 7(2), 2688-2706. DOI: 10.15376/biores.7.2.2688-2706
- Terinte, N., Ibbett, R., and Schuster, K. C. (2011). "Overview on native cellulose and microcrystalline cellulose I structure studied by X-ray diffraction (WAXD): Comparison between measurement techniques," *Lenzinger Berichte* 89, 118-131.
- Uesu, N. Y., Pineda, E. A. G., and Hechenleitner, A. A. W. (2000). "Microcrystalline cellulose from soybean husk: Effects of solvent treatments on its properties as acetylsalicylic acid carrier," *International Journal of Pharmaceutics* 206(1), 85-96. DOI: 10.1016/S0378-5173(00)00532-9
- Zhao, J., Zhang, H., Zheng, R., Lin, Z., and Huang, H. (2011). "The enhancement of pretreatment and enzymatic hydrolysis of corn stover by FeSO<sub>4</sub> pretreatment," *Biochemical Engineering Journal* 56(3), 158-164. DOI: 10.1016/j.bej.2011.06.002

Article submitted: August 8, 2014; peer review completed: October 2, 2014; Revised version received: October 10, 2014; Accepted: October 14, 2014; Published: October 23, 2014.